ACS APPLIED BIO MATERIALS

www.acsabm.org Article

Near-Infrared Visualization of NAD(P)H Dynamics in Live Cells and *Drosophila melanogaster* Larvae Using a Coumarin-Based Pyridinium Fluorescent Probe

Sophia Jaeger, Henry Lanquaye, Sushil K. Dwivedi,* Dilka Liyana Arachchige, James Xia, May Waters, Bella Lyn Bigari, Adenike Mary Olowolagba, Peter Agyemang, Yang Zhang, Yan Zhang,* Athar Ata,* Ishana Kathuria, Rudy L Luck,* Thomas Werner, and Haiying Liu*

Cite This: *ACS Appl. Bio Mater.* 2024, 7, 8465−8478 Read Online

ACCESS | Metrics & More | Article Recommendations | Supporting Information

ABSTRACT: A near-infrared fluorescent probe, **A**, was designed by substituting the carbonyl group of the coumarin dye's lactone with a 4-cyano-1-methylpyridinium methylene group and then attaching an electron-withdrawing NADH-sensing methylquinolinium acceptor via a vinyl bond linkage to the coumarin dye at the 4-position. The probe exhibits primary absorption maxima at 603, 428, and 361 nm, and fluoresces weakly at 703 nm. The addition of NAD(P)H results in a significant blue shift in the fluorescence peak from 703 to 670 nm, accompanied by a substantial increase in fluorescence intensity. This spectral shift is attributed to the transformation from an A−π−A−π−D configuration to a D−π−A−π−D pyridinium platform in probe **AH**, owing to the addition of a hydride from NADH to the electron-accepting quinolinium acceptor producing the electron-contributing 1-methyl-1,4-dihydroquinoline donor in probe **AH**. This conclusion is supported by theoretical calculations. The probe was utilized to investigate NAD(P)H dynamics under various conditions. In HeLa cells, treatment with glucose or maltose resulted in a substantial elevation in near-infrared emission intensity, suggesting increased NAD(P)H levels. Chemotherapeutic agents including cisplatin and fludarabine at concentrations of 5, 10, and 20 μM brought about a dose-dependent increase in emission intensity, reflecting heightened NAD(P)H levels due to drug-induced stress and cellular damage. In vivo experiments with hatched, starved *Drosophila melanogaster* larvae were also conducted. The results showed a clear relationship between emission intensity and the levels of NADH, glucose, and oxaliplatin, confirming that the probe can detect variations in NAD(P)H levels in a living organism. Our investigation also demonstrates that NAD(P)H levels are significantly elevated in the cystic kidneys of ADPKD mouse models and human patients, indicating substantial metabolic alterations associated with the disease. This near-infrared emissive probe offers a highly sensitive and specific method for monitoring NAD(P)H levels across cellular, tissue and whole-organism systems. The ability to detect NAD(P)H variations in reaction to varying stimuli, including nutrient availability and chemotherapeutic stress, underscores its potential as a valuable resource for biomedical research and therapeutic monitoring.

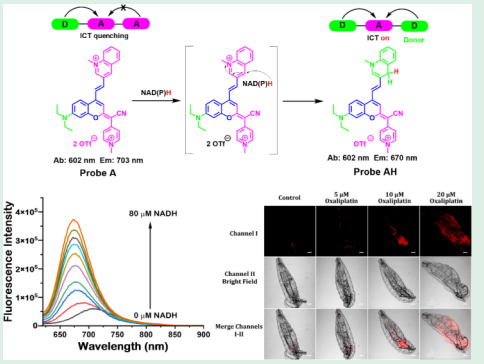

KEYWORDS: *near-infrared imaging, fluorescent probe, NAD(P)H, coumarin, fruit fly larvae, HeLa cells*

1. INTRODUCTION

NADH (nicotinamide adenine dinucleotide) alongside NADPH (its phosphate variant) are vital cofactors that significantly influence cellular metabolism, energy transfer, and overall cellular function.[1−8] These molecules play key roles in various metabolic pathways: NADH is integral to catabolic processes, where it facilitates the conversion of nutrients into ATP, the primary energy currency of the cell. This process not only provides energy but also supports the synthesis of essential biomolecules. On the other hand, NADPH is crucial for anabolic reactions, including lipid and nucleic acid synthesis, and acts as a reducing agent in cellular antioxidant defenses, helping to neutralize reactive oxygen species and protect cellular integrity. The levels of NAD(P)H are tightly regulated and reflect the metabolic state of the cell. Alterations in these cofactors are associated with numerous pathological conditions, such as chronic kidney disease, cancer, cardiovascular diseases, metabolic disorders, mitochondrial dysfunction, liver disease, and neurodegenerative diseases.[1−8] These changes can profoundly affect cellular metabolism, signaling pathways, and energy homeostasis, further emphasizing the

Received: September 8, 2024
Revised: November 4, 2024
Accepted: November 8, 2024
Published: November 19, 2024

https://doi.org/10.1021/acsabm.4c01294
ACS Appl. Bio Mater. 2024, 7, 8465−8478

Scheme 1. Near-Infrared Coumarin-Based Emissive Probe for NAD(P)H Sensing in Live Cells

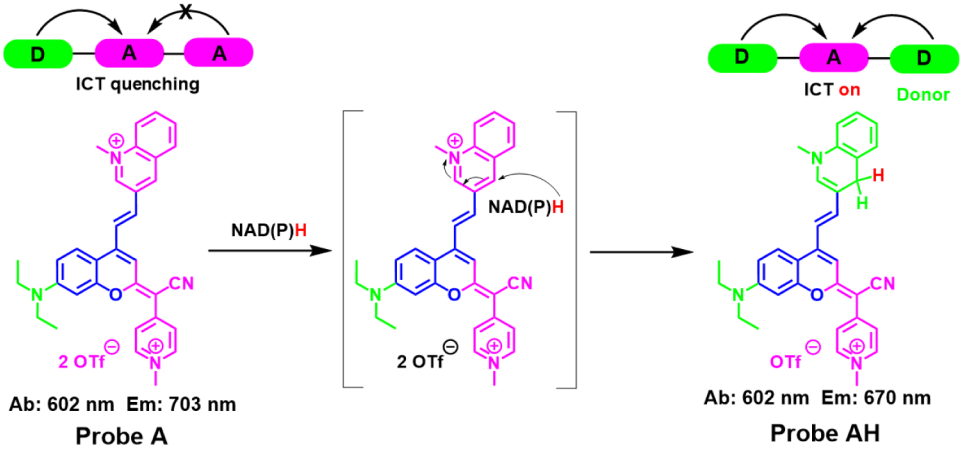

need for precise and real-time monitoring of NAD(P)H dynamics. Understanding the intricate roles of NAD(P)H in cellular metabolism and energy transfer is essential for linking these cofactors to cellular health and function. This knowledge not only enhances our comprehension of metabolic regulation but also provides valuable insights into the mechanisms underlying disease progression, paving the way for potential therapeutic interventions aimed at restoring metabolic balance. Therefore, accurate and live monitoring of NADH and NADPH dynamics is essential for understanding cellular metabolism, redox signaling, and disease progression.[1−8] Traditional methods for analyzing NADH and NADPH often lack the spatial and temporal resolution needed for detailed studies within live cells. Techniques such as spectrophotometry and enzyme-coupled assays may not capture the nuanced dynamics of these cofactors in complex cellular environments. To address these limitations, the synthesis of fluorescent probes capable of selectively detecting NAD(P)H has emerged as a powerful strategy (Table S1).[7−24] Near-infrared (NIR) fluorescent probes offer distinct advantages over conventional fluorescent methods.[9,16,19,21,23,24] They provide superior tissue penetration and reduced background autofluorescence, which are critical for in vivo imaging and dynamic studies in live cells. Furthermore, while NADH exhibits fluorescence at 450 nm and absorption at 350 nm, NIR probes can avoid interference by operating in a different spectral range, thus enhancing specificity and sensitivity.[9,16,19,21,23,24] Coumarin-based fluorophores are well-suited for biological applications owing to their high molar absorptivity, excellent photostability, and low cytotoxicity.[25−29] The high molar absorptivity of coumarins enables sensitive detection with minimal probe concentrations, while their excellent photostability ensures reliable and consistent performance over time. Coumarins also provide the flexibility needed to fine-tune photophysical properties, which is essential for designing probes with high selectivity for specific biomolecules like NADH and NADPH.[25−38] Moreover, coumarin derivatives are cost-effective and easily synthesized, making them practical for both research and clinical use.[25−38]

In this study, we introduce a NIR emissive probe designed for the selective determination of NAD(P)H. The probe incorporates a NAD (P)H-sensing methylquinolinium acceptor linked via a vinyl bond to a coumarin dye at the 4-position and features a 4-cyano-1-methylpyridinium methylene group that replaces the carbonyl of the coumarin dye's lactone moiety (Scheme 1). The probe exhibits absorption peaks at 603, 428, and 361 nm and a weak emission peak at 703 nm. Upon reaction with NAD(P)H, the emission shifts significantly from 703 to 670 nm, with a marked increase in intensity. This shift is due to the transition from an A−π−A−π−D to a D−π−A−π−D pyridinium configuration, driven by the NADH-triggered reduction of the methylquinolinium electron-pulling acceptor to a 1-methyl-1,4-dihydroquinoline electron-rich donor. We validated the probe's capabilities by studying NAD(P)H dynamics under various treatment conditions. In HeLa cells, glucose and maltose treatments led to increases in near-infrared emission intensity, reflecting augmented NAD(P)H levels. Furthermore, treatment with cisplatin and fludarabine at 5, 10, and 20 μM concentrations resulted in dose-proportional increases in emission intensity, revealing enhanced NAD(P)H levels due to drug-triggered cellular stress. In vivo experiments with developed starved *Drosophila* larvae further confirmed the probe's effectiveness. The larvae, exposed to varying concentrations of NADH, glucose, and oxaliplatin, revealed a direct link between emission intensity and the levels of these substances. This supports the probe's capability to determine NAD(P)H changes in live organisms. Overall, this NIR fluorescent probe provides a highly sensitive and specific method for monitoring NAD(P)H levels, leveraging the high molar absorptivity and excellent photostability of coumarin-based fluorophores. Its ability to circumvent fluorescence interference from NADH and respond dynamically to metabolic changes highlights its potential as a valuable tool for biomedical research and therapeutic monitoring.

2. EXPERIMENTAL SECTION

Please see the detailed information in Supporting Information.

3. RESULTS AND DISCUSSION

3.1. The Design and Construction of the Probe.

Coumarin derivatives have garnered attention as versatile platforms for fluorescent probe design due to their inherent fluorescence properties and structural variability.[25−38] The absorption and emission wavelengths of coumarin dyes can be fine-tuned through chemical modifications, making them suitable for applications in both visible and near-infrared (NIR) regions.[25−38] This study focused on developing a NIR probe for NAD(P)H detection using a coumarin derivative. We designed a probe by incorporating 3-quinolinium acceptor

https://doi.org/10.1021/acsabm.4c01294
ACS Appl. Bio Mater. 2024, 7, 8465−8478

Scheme 2. Synthesis of a Near-Infrared Coumarin-Based Fluorescent Probe for NAD(P)H Detection

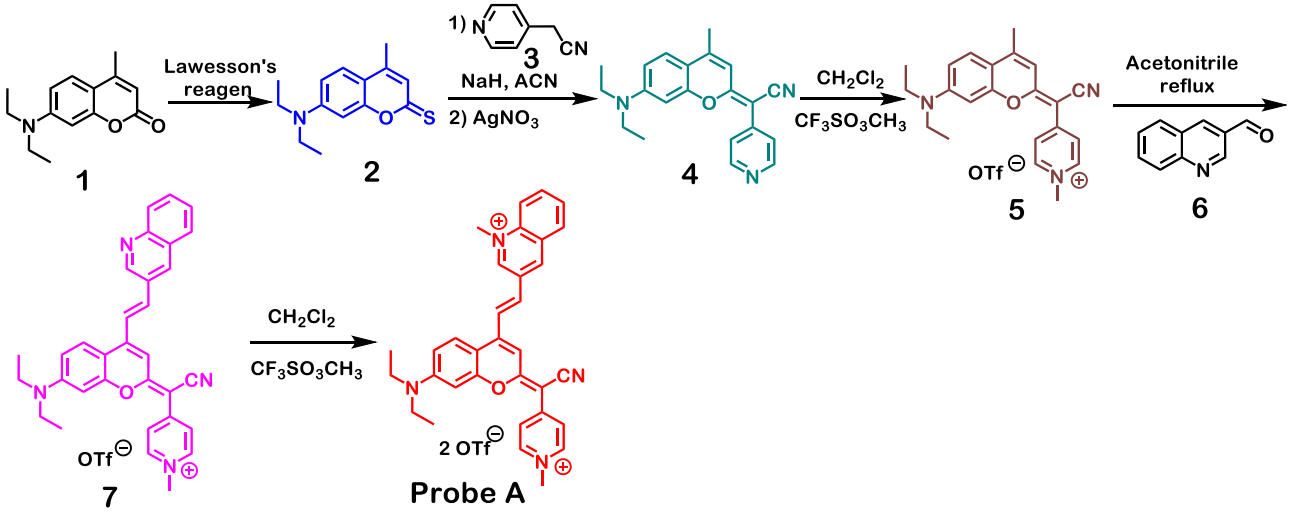

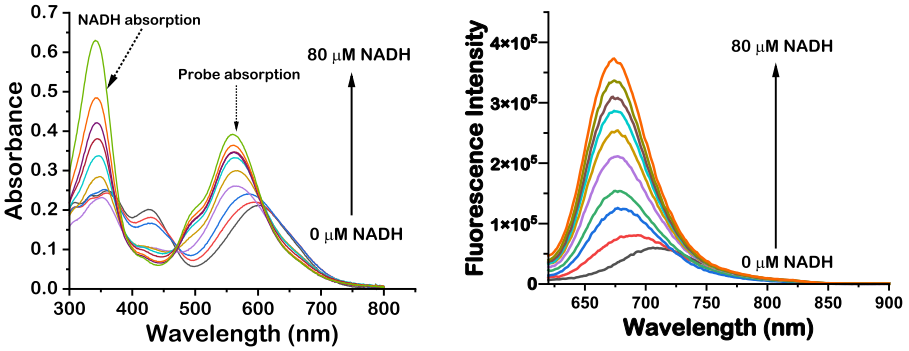

Figure 1. Optical spectra of probe **A** with 5 μM in PBS buffer at pH 7.4 supplemented with 5% DMSO, both without and with varying NADH concentrations over a period of 60 min under 600 nm excitation.

via a vinyl bond linkage to the coumarin dye at the 4-position, while simultaneously substituting the carbonyl of the lactone function with 4-cyano-1-methylpyridinium methylene functionality to enhance electron-withdrawing feature within the probe. These structural modifications were hypothesized to confer NIR emission properties to the probe and enhance its sensitivity and selectivity toward NAD(P)H. The synthesis of the probe commenced with readily available starting materials such as 7-(diethylamino)-4-methyl-2*H*-chromen-2-one (**1**). Initially, we synthesized thiocoumarin (**2**) through the reaction of compound **1** with Lawesson's reagent. Subsequently, compound **2** reacted with 4-pyridylacetonitrile, yielding (*E*)-2-(7-(diethylamino)-4-methyl-2*H*-chromen-2-ylidene)-2-(pyridin-4-yl)acetonitrile (**4**). This intermediate was then subjected to methylation, leading to the formation of compound **5**. A condensation reaction between compound **5** and quinoline-3-carbaldehyde (**6**) afforded compound **7**, which underwent further methylation to yield the final probe (Scheme 2). The final compound was characterized by diverse spectroscopic techniques, confirming its chemical structure and purity (Figures S1−S6).

3.2. Optical Behavior of the Probe in the Presence of NADH. The spectral characteristics of a probe serve as a powerful tool for understanding its optical behavior, both in the presence and absence of NADH. Initially, in the absence of NADH, the probe demonstrates distinct absorption peaks at 603, 428, and 361 nm. These peaks align with specific molecular components within the probe, with the 603 nm peak attributed to the extensive pi-conjugation of the coumarin-based pyridinium dye, the 428 nm peak stemming from transmission from the coumarin section, and the 361 nm peak associated with the presence of the 3-quinolinium moiety. The addition of NADH to solutions of the probe in buffer solution at pH 7.4 results in significant changes in the absorption spectrum. First, there is a noticeable blue shift in the absorption peak from 603 to 559 nm, indicative of the structural transformation caused by the addition of a hydride from the reaction with NADH. This shift is complemented by a gradual reduction in the absorption peak at 428 nm, also suggestive of a modification or interaction involving the coumarin component of the probe (Scheme 1). Additionally, the absorption peak at 345 nm increases significantly due to NADH absorption. In a fluorescence experiment under excitation at 600 nm, the probe shows a weak near-infrared peak at 703 nm without NADH. However, upon gradual addition of NADH to the probe buffer solution, fluorescence intensification is observed, accompanied by a notable blue shift of the fluorescence spectra. This blue shift is evident as the near-infrared emission peak transitions from 703 to 670 nm (Figure 1, right). This intriguing change results from the establishment of a distinct D−π−A−π−D hemicyanine platform from A−π−A−π−D via NADH-triggered transformation of the quinolinium electron-deficient acceptor into the electron-donative 1-methyl-1,4-dihydroquinoline donor.

https://doi.org/10.1021/acsabm.4c01294
ACS Appl. Bio Mater. 2024, 7, 8465−8478

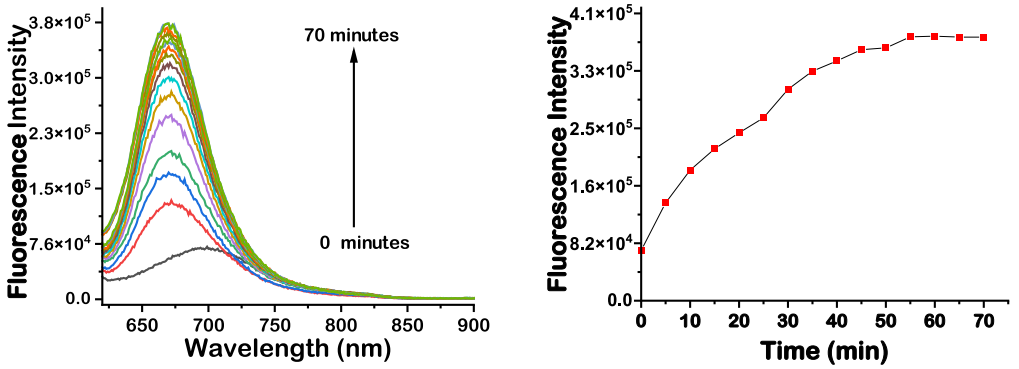

Figure 2. Emission spectra of probe **A** with 5 μM in PBS buffer at pH 7.4 supplemented with 5% DMSO and 80 μM NADH, incubated for 70 min under 600 nm excitation.

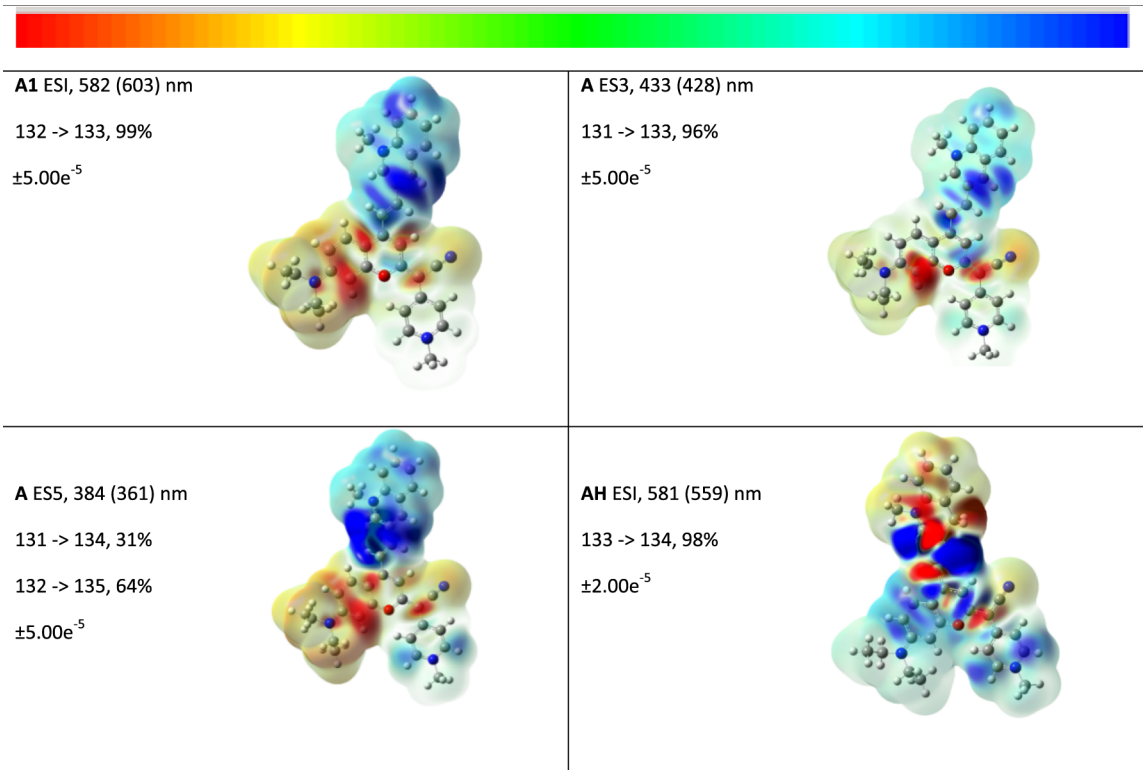

Figure 3. Current density difference diagrams for the electronic transitions as isosurfaces for probes **A** (ES1, 3, and 5) and **AH** (ES1). The figure displays the number of the excited state (ES) along with the calculated and experimental wavelengths, as well as the associated transitions and their contribution percentages. The color scale range values are indicated at the top of the figure. Detailed drawings of the numbered linear combination of atomic orbitals are provided in the Supporting Information.

This reaction underscores the complex interplay of molecular interactions driving the observed spectral shifts, providing deeper insights into the probe's behavior in the presence of NADH. The addition of a hydride ligand to probe A resulting in the formation of AH was also confirmed by molecular weight determinations using an electrospray mass spectrometer (Figure S6). The probe displayed stable fluorescence responses for 60 min (Figure 2) and was stable under excitation in the presence of 80 μM NADH for 2 h, Figure S9.

3.3. Theoretical Calculations. The geometries of the probe were optimized using the Gaussian 16 program[39] with the APFD functional[40] and with atoms identified by the 6-311+G(d,p) basis set. These calculations were carried out to investigate the electronic absorption characteristics and geometry of the probes **A** and **AH**. In Probe **A**, Figures 3 and S11, the planar coumarin and quinolinium moieties are arranged at an interplanar angle of around 36.9°, implying limited π-conjugation between the two moieties. Probe **AH**, Figures 3 and S15, looks roughly coplanar but is also twisted slightly near the quinoline moiety at 16.5° suggesting a greater degree of conjugation of the coumarin and quinolinium moieties compared to probe **A**.

Probe **A** displayed three absorptions calculated theoretically, 582, 433, and 384 nm, corresponding to excited states (ES) 1, 3, and 5, respectively, Figures 3 and S19, in good agreement with those observed experimentally centered at 603, 428, and 361 nm, Figure 1. As can be seen in Figure S19 the calculated absorption near ES 5 also had contribution from another transition, i.e., ES 6, calculated to be at 359 nm, resulting in an overall absorption at 370 nm. The current density illustration

https://doi.org/10.1021/acsabm.4c01294
ACS Appl. Bio Mater. 2024, 7, 8465−8478

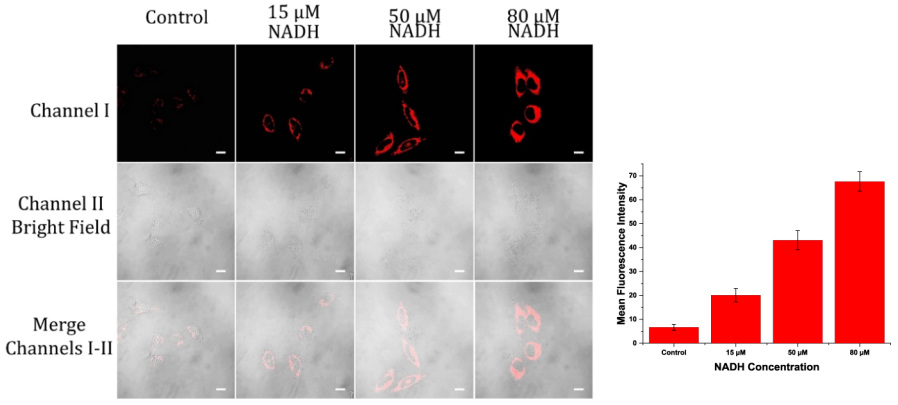

Figure 4. Emission images of HeLa cells exposed to NADH concentrations (0, 15, 50, and 80 μM) in glucose-deficient DMEM for 30 min, and then incubated probe **A** with 5 μM in glucose-deficient DMEM for 30 min. Emission was measured within the 650−750 nm emission range utilizing excitation at 559 nm.

for this transition shown in Figure S22 is similar to that depicted for ES5, Figure 3. Excited states 1, 3, 5, and 6 involve movement of electron density from the coumarin section of probe **A** to the electron-deficient quinolinium moiety but the higher energy ES 5 and 6 also contained some transfer to the pyridinium section of the probe.

The calculated UV spectrum for probe **AH**, Figure S24, differed from that for probe **A** in that one major absorption was observed at 581 nm close to the 559 nm observed experimentally. The calculated spectrum, Figure S24, also did not contain an absorption at 428 nm as did probe **A,** and the reason for this is now made clear. The addition of the hydride ligand to the quinolinium moiety produced an electron-rich region here and thus the electronic transition consisted of movement of electron density from this quinolinium region to the central coumarin and the pyridinium moieties as depicted in the current density illustration in Figure 3. The absorption at 428 nm for probe **A** involved electron density moving in the opposite direction and this is not possible for probe **AH**, Figure 3.

3.4. Evaluation of Probe Selectivity, Stability, and Cytotoxicity. Probe **A** demonstrates exceptional selectivity toward NAD(P)H when contrasted with a diverse range of compounds. Various cations (such as Co^{2+}, K^+, Na^+, Fe^{3+}, and Ca^{2+}), anions (including Cl^-, HCO_3^-, NO_2^-, and NO_3^-), amino acids (comprising cysteine, glutathione, DL-tyrosine, methionine, and lysine), and carbohydrates (such as ribose, glucose, lactate, pyruvate, and fructose) do not result in an increase in fluorescence over the control (Figure S8). This heightened degree of specificity is of significant consequence for accurately identifying and quantifying NAD(P)H, a pivotal coenzyme crucial for energy metabolism and a range of cellular activities. Probe **A**'s unique ability to discriminate NAD(P)H precisely, while avoiding interference due to other substances, facilitates the precise determination of this essential molecule in elaborate biological samples.

The capacity to resist photobleaching or emission loss from prolonged illumination, often termed photostability, is an essential characteristic of fluorescent dyes. The noteworthy photostability of the probe **A** is demonstrated by minimal changes in fluorescence even after continuous excitation for 2 h at 600 nm. This stability is vital for procedures that involve prolonged or frequent imaging, since photobleaching can compromise signal fidelity and image accuracy. The strong photostability displayed by probe **A** makes it invaluable for applications that require consistent and reliable fluorescence measurements for imaging and detection purposes (Figure S9).

To evaluate probe **A**'s potential toxicity, an MTT-based viability test following established protocols as detailed in the Supporting Information was conducted. HeLa cells were subjected to probe **A** for 24 h, and the conversion of MTT dye from yellow to purple in the mitochondria, which indicates cell viability was monitored.[31,41−46] Our results reveal that at a concentration of 50 μM, cells maintain a viability level above 85%, suggesting that some cytotoxicity was induced by the probe (Figure S10). Employing probes with low cytotoxicity is vital to prevent negative impacts on cellular function, thereby ensuring the accuracy of experimental outcomes. Additionally, low probe cytotoxicity facilitates extended exposure periods or repetitive measurements, both of which are indispensable for extended-duration studies and observing treatment responses.

3.5. Selective Fluorescence Response of the Probe to Cellular NAD(P)H Levels. To study the selective fluorescence response of probe **A** to cellular NAD(P)H levels, we employed it to monitor dynamic variations in NAD(P)H under various chemical treatments. Probe **A** is activated by near-infrared emission and is highly selective for NAD(P)H, making it a suitable tool for this purpose. Control experiments were initially performed using HeLa cells, where 5 μM probe **A** was applied in glucose-restricted DMEM for 30 min, with no prior NADH exposure. The cells exhibited minimal fluorescence in these baseline conditions (Figure 4), implying minimal inherent NADH levels. This outcome reveals that probe **A** does not respond without elevated NADH levels, confirming its specificity. Subsequently, we executed NADH dose−response testing with HeLa cells. The cells were incubated with different NADH concentrations for 30 min in glucose-deficient DMEM prior to exposure to probe **A** (Figure 4). The observations displayed a marked increase in emission intensity corresponding to the dose of NADH. Progressively higher emission intensity was observed with increasing NADH pretreatment concentrations, correlating directly with the NADH levels in the extracellular environment. The concentration-related emission response reinforces the specificity of probe **A** for detecting NADH levels within the cells. The increased emission fluorescence intensity with elevated NADH content further validates probe **A**'s capacity to selectively respond to NADH. These observations from control and dose−response experiments establish that probe **A** effectively monitors NADH fluctuations with high specificity, avoiding

https://doi.org/10.1021/acsabm.4c01294
ACS Appl. Bio Mater. 2024, 7, 8465−8478

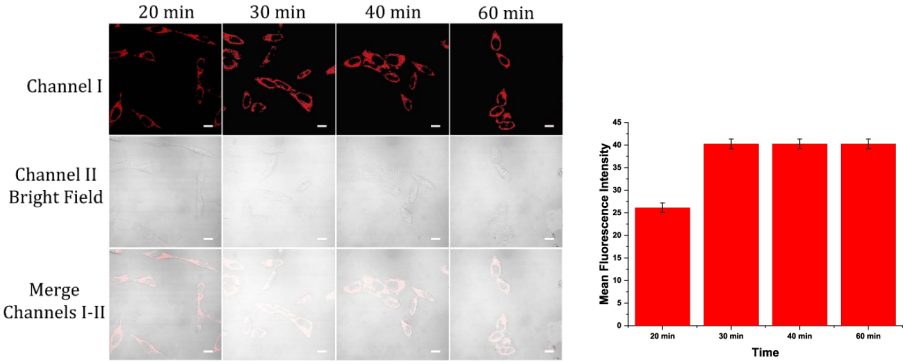

Figure 5. Emission images of HeLa cells underwent exposure to 50 μM NADH in glucose-deficient DMEM for time intervals of 20, 30, 40, and 60 min, subsequent to a 30 min treatment of 5 μM probe **A** in glucose-deficient DMEM. Emission was measured within the 650−750 nm emission range utilizing excitation at 559 nm.

irrelevant activation. Similar results were obtained using A549 fibroblast cells, further validating the probe's performance (Figures S12 and S13). The significant association between NADH levels and emission intensity of the probe supports accurate quantitative imaging, providing crucial understanding of redox metabolism and energy regulation in viable cells (Figure 4). This specificity and sensitivity make probe **A** a crucial asset for investigating cellular metabolic processes and responses to various treatments.

To assess the fluorescence responsiveness of probe **A** in live HeLa cells, we assessed the probe's ability to detect NADH at various incubation times. HeLa cells underwent exposure to 50 μM NADH in glucose-deficient DMEM, and subsequently, probe **A** (5 μM) was introduced for 30 min. Confocal fluorescence microscopy was employed to capture fluorescence images at different time points: 20, 30, 40, and 60 min post-NADH treatment. The results reveal that fluorescence intensity from probe **A** increases in response to NADH treatment (Figure 5). Notably, the fluorescence intensity reaches a steady state at the 30 min mark. This indicates that probe **A** effectively detects NADH within this time frame, achieving optimal fluorescence signal. Further observations show that extending the incubation period to 40 and 60 min does not result in significant changes in fluorescence intensity. This plateau in fluorescence intensity suggests that the probe's responsiveness is maximized at 30 min, and additional incubation time does not enhance or diminish the signal. These findings underscore the efficiency of probe **A** in providing a stable and reliable fluorescence signal for NADH detection within a specific time frame. The steady response at 30 min highlights the probe's suitability for live tracking of NADH dynamics in cellular environments. The lack of significant changes in fluorescence at longer incubation times indicates that probe **A** reaches equilibrium with NADH in approximately 30 min, making it a valuable tool for precise and reproducible measurements of NADH levels in live cells. Overall, these results confirm that probe **A** offers a consistent and effective approach for monitoring NADH levels, providing essential insights into cellular metabolic processes and the dynamics of redox reactions. The probe's performance within this time frame enhances its utility for real-time fluorescence imaging in various experimental settings.

3.6. Mitochondria-Specific Targeting of the Probe. Probe **A** with a single positive charge should achieve selective electrostatic interaction-based mitochondrial targeting in live cells. Mitochondria are characterized by a negatively charged membrane potential relative to the cytosol, which attracts positively charged molecules. To validate the hypothesis that our probe would localize specifically to mitochondria, we performed a colocalization analysis using HeLa cells (Figure 6). After pretreatment of HeLa cells with 50 μM of NADH for

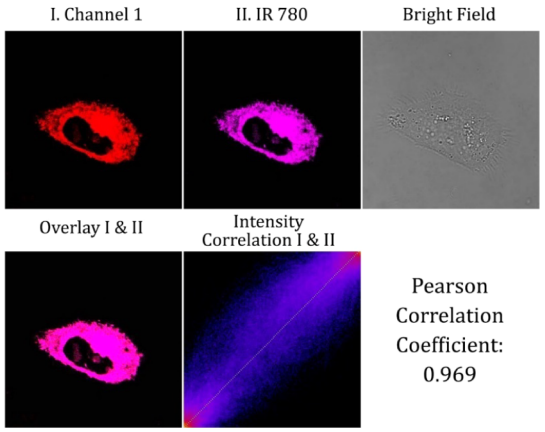

Figure 6. Emission microscopy images of HeLa cells treated with 50 μM NADH in glucose-deficient DMEM for 30 min, subsequent to a 30 min treatment of 5 μM probe **A** and 5 μM IR-780 in glucose-depleted DMEM for a further 30 min. Emission from probe **A** was detected in the 650−750 nm range with 559 nm excitation, while IR-780 emission was captured between 750−800 nm with the same excitation wavelength.

30 min, the cells were then coincubated with probe **A** and the mitochondria-selective dye IR-780 for 30 min. Fluorescence microscopy was used to observe the localization of both probe **A** and IR-780. The imaging data indicated a pronounced overlap in the emission signals of both dyes. To quantify the degree of colocalization, we calculated the Pearson correlation coefficient, a standard metric for assessing the overlap between fluorescence signals (Figure 6). The coefficient was greater than 0.96, indicating a substantial correlation between the fluorescence of probe **A** and IR-780 within the mitochondria. This high coefficient suggests that probe **A** is predominantly localized within the mitochondria. The positive charge on probe **A** is likely instrumental in its mitochondrial targeting, as this would be facilitated by the electrostatic attraction to the mitochondria's negatively charged membrane potential. This interaction promotes the probe's accumulation within mitochondria, given the strong electrochemical gradient across

https://doi.org/10.1021/acsabm.4c01294
ACS Appl. Bio Mater. 2024, 7, 8465−8478

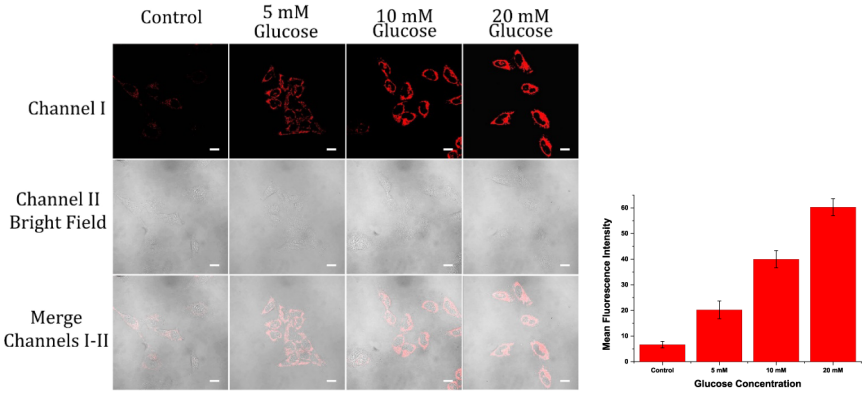

Figure 7. Emission images of HeLa cells treated with altered glucose concentrations in glucose-deficient DMEM for 30 min, subsequent to a 30 min treatment of 5 μM probe **A** in glucose-deficient DMEM. Emission was measured in the 650−750 nm range with 559 nm excitation.

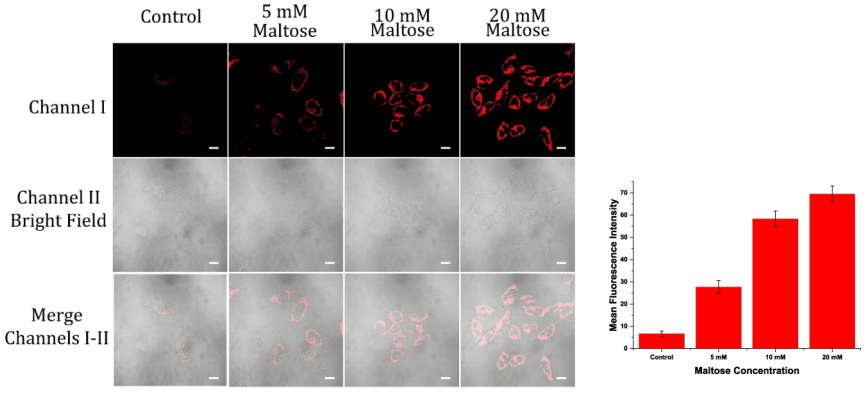

Figure 8. Emission images of HeLa cells pretreated with maltose at various concentrations (0, 5, 10, and 20 mM) for 30 min, subsequent to a 30 min treatment of 5 μM probe **A** in glucose-deficient DMEM. Emission was captured in the 650−750 nm range with 559 nm excitation.

the membrane of the mitochondria that favors the entry and retention of positively charged molecules. This was further validated by colocalization experiments conducted in A549 cells (Figure S14). These results demonstrate that probe **A** not only detects NAD(P)H content but also exhibits selective mitochondrial localization, making it a valuable tool for studying mitochondrial dynamics.

3.7. Mapping the Flux of Cellular NAD(P)H under Diverse Chemical Conditions. Glucose is a critical component of cellular metabolism, serving as a primary substrate for glycolysis, which in turn produces NADH, a vital molecule for energy production and redox reactions.[47] Elevated glucose levels typically boost glycolytic activity, leading to increased NAD(P)H production. Understanding how varying glucose concentrations influence NAD(P)H levels can provide valuable insights into cellular metabolic processes and energy regulation. In our study, HeLa cells were first exposed to altered glucose levels for 30 min to investigate this relationship. Following this treatment, the cells experienced an additional 30 min incubation with 5 μM probe **A** in glucose-deficient DMEM. The confocal fluorescence microscopy images, as shown in Figure 7, illustrate the impact of glucose concentration on NAD(P)H levels within HeLa cells. The control group (0 mM glucose) displayed minimal fluorescence, reflecting low basal NAD(P)H levels. In contrast, increasing glucose concentrations produced an incremental increase in emission intensity. Specifically, as glucose concentrations rose, emission levels also increased, indicating a direct correlation between glucose availability and NAD(P)H production. These findings demonstrate that probe **A** effectively detects variations in NAD(P)H levels triggered by glucose availability. Tracking NAD(P)H variations with respect to glucose levels provides an improved understanding of cellular energy metabolism and glucose's effects on cellular processes.

Probe **A** was also employed to elucidate how maltose influences NAD(P)H levels in HeLa cells. Maltose, a disaccharide sugar that hydrolyzes into glucose, plays a crucial role in cellular metabolism by increasing glucose availability. This increase in glucose can subsequently affect NAD(P)H levels, as glucose is a key substrate for metabolic pathways involving NAD(P)H. HeLa cells were subjected to pretreatment with a range of concentrations of maltose for 30 min to simulate different levels of glucose availability. Following maltose treatment, the cells received a 30 min exposure to 5 μM probe **A** in glucose-deficient DMEM to measure NAD (P) H levels. The emission imaging results reveal a clear dose-replated increase in NAD (P)H levels resulting from maltose treatment. In the absence of maltose (0 mM), emission intensity was minimal, indicating low baseline levels of NAD(P)H. Since maltose concentrations increased, emission intensity progressively rose, with the most substantial increase observed at 20 mM maltose. Specifically, maltose concentrations of 5 mM and 10 mM brought about moderate fluorescence increases, which became more pronounced at higher concentrations (Figure 8). The dose-dependent response observed with probe **A** highlights its utility in monitoring metabolic fluctuations, offering valuable informa-

https://doi.org/10.1021/acsabm.4c01294
ACS Appl. Bio Mater. 2024, 7, 8465−8478

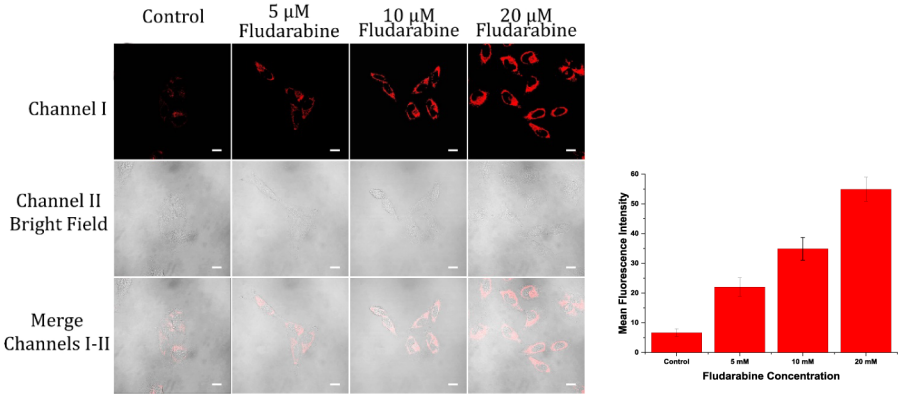

Figure 9. Emission images of HeLa cells treated with fludarabine at concentrations of 0, 5, 10, and 20 μM in glucose-deficient DMEM for 30 min, followed by an additional 30 min application of 5 μM probe **A**. Emission was detected in the 650−750 nm emission range with a 559 nm excitation.

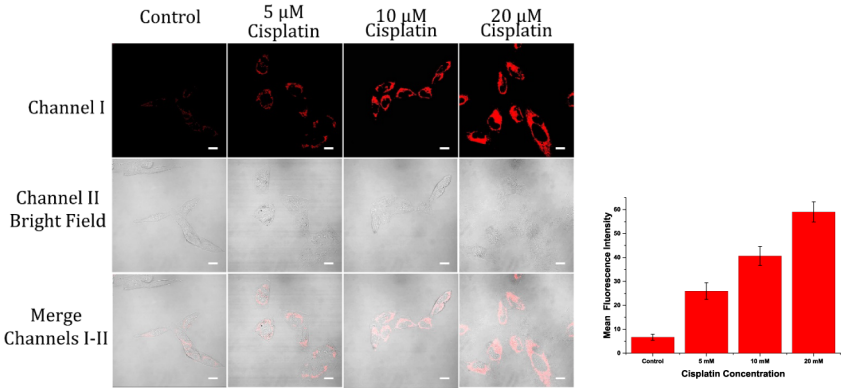

Figure 10. Emission images of HeLa cells pretreated with cisplatin at 0, 5, 10, and 20 μM concentrations in glucose-deficient DMEM for 30 min, subsequent to a 30 min treatment of 5 μM probe **A** in glucose-deficient DMEM. Emission was imaged in the 650−750 nm range with 559 nm excitation.

tion for research into cellular metabolism and related biological processes.

Fludarabine, a chemotherapeutic agent used primarily for treating various types of leukemia and lymphomas, is known to induce significant cellular stress and damage.[48−50] This drug also induces apoptosis through different mechanisms, including interference with DNA synthesis and repair.[48−50] To study how fludarabine influences NAD(P)H levels, we carried out an experiment with HeLa cells subjected to varying concentrations of fludarabine in glucose-deficient DMEM for 30 min. After treatment, cells underwent an extra 30 min treatment with 5 μM probe **A** in glucose-deficient DMEM (Figure 9). This experiment was designed to elucidate the impact of fludarabine on NAD(P)H levels, given that chemotherapeutic agents like fludarabine can induce oxidative stress and alter cellular redox states. Fludarabine's mechanism of action involves disrupting DNA synthesis and repair, leading to increased oxidative stress and altered metabolic processes. This stress can trigger changes in NAD(P)H levels as part of the cellular response to counteract the induced damage. The confocal microscopy images reveal a clear dose-related enhancement in emission intensity correlating with fludarabine concentration. The control group (0 μM fludarabine) showed minimal fluorescence, indicating low NAD(P)H levels under basal conditions. In contrast, cells administered fludarabine exhibited progressively higher fluorescence intensities. The documented increase in fluorescence intensity is indicative of enhanced NAD(P)H production or accumulation, likely due to the oxidative stress and disruption of cellular redox balance caused by fludarabine. As cells experience increased stress and damage, they may upregulate NAD(P)H production to mitigate oxidative stress and support cellular repair mechanisms. Overall, these findings confirm that probe **A** is effective in detecting variations in NAD(P)H levels resulting from fludarabine treatment.

Cisplatin serves as a frequently administered chemotherapy drug known for its effectiveness in treating various cancers.[51−54] It works primarily by inducing DNA cross-linking and cellular stress, which can disrupt normal cellular functions and redox balance.[51−54] Comprehending cisplatin's impact on NAD(P)H levels is vital for uncovering its role in cellular metabolism and stress response pathways. We investigated these effects by treating HeLa cells with diverse concentrations of cisplatin in glucose-deficient DMEM for 30 min. Subsequently, an extra 30 min treatment was performed with 5 μM probe **A** in glucose-deficient DMEM. The emission images shown in Figure 10 reveal a distinct increase in emission intensity that correlates with the dose of cisplatin treatment. The control group (0 μM cisplatin) showed minimal fluorescence, corresponding to low NAD(P)H levels. In comparison, HeLa cells exposed to cisplatin levels of 5, 10, and 20 μM exhibited progressively higher fluorescence intensities. This emission intensity increase reflects an elevation in NAD(P)H levels within the cells because of cisplatin treatment. Given cisplatin's role in inducing cellular stress and damage, it is plausible that the observed increase in

https://doi.org/10.1021/acsabm.4c01294
ACS Appl. Bio Mater. 2024, 7, 8465−8478

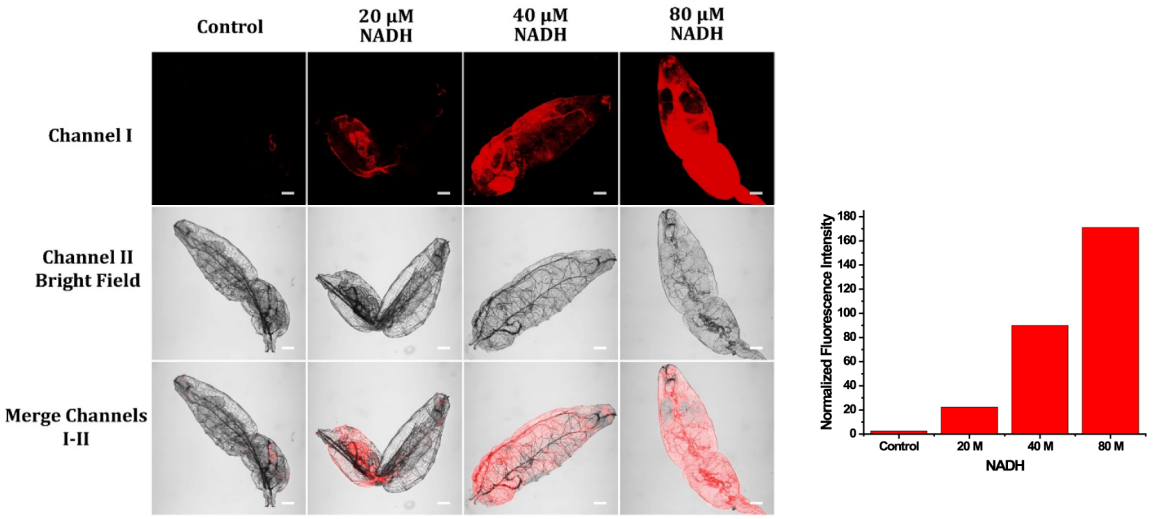

Figure 11. Emission images of hewly hatched, food-deprived fly larvae pretreated with diverse NADH concentrations in pH 7.4 phosphate-buffer for 2 h. Afterward, the larvae were subjected to three PBS washes and incubated with probe **A** at 10 μM in a PBS for an extra 2 h. Emission was imaged in the 650−750 nm range with 559 nm excitation.

NAD(P)H reflects a compensatory response to oxidative stress. Cisplatin can induce metabolic alterations, including enhanced glycolysis and increased NAD(P)H production, as cells attempt to counteract the stress and maintain redox balance.[51−54] By using probe **A**, which specifically responds to alterations in NAD(P)H levels, we can detect these fluctuations and gain insights into how cisplatin influences cellular metabolism. These findings provide valuable information on how cisplatin impacts cellular redox states and metabolic processes, enhancing our understanding of the drug's effects and its role in therapeutic interventions.

TGF-beta (transforming growth factor beta) is a multifunctional cytokine essential for cell growth, differentiation, and tissue repair. The upsurge in NAD(P)H levels we observed aligns with TGF-beta's established role in enhancing energy metabolism in fibroblasts. Specifically, TGF-beta activates signaling pathways that promote glycolysis and mitochondrial function, thereby meeting the energy demands of cellular proliferation and differentiation. This metabolic shift likely indicates heightened biosynthetic activity necessary for extracellular matrix production and tissue remodeling. To further investigate the impact of TGF-beta on fibroblast cells, we performed confocal fluorescence microscopy to analyze cellular responses to TGF-beta concentrations of 0 ng/mL and 10 ng/mL. After a 30 min exposure, The cells received a further 30 min of incubation with probe **A**. As shown in Figure S15, TGF-beta-treated fibroblast cells exhibited a substantial increase in fluorescence intensity in comparison to the control group, indicating elevated NAD(P)H levels. This suggests that TGF-beta stimulates metabolic activity and alters cellular redox states. Our findings demonstrate that TGF-beta significantly influences the metabolic state of fibroblast cells, as evidenced by the increased NAD(P)H levels detected with probe **A**. These results highlight TGF-beta's critical role in regulating cellular metabolism and its implications for conditions such as fibrosis. Future research should focus on elucidating the specific signaling pathways involved and their broader effects on fibroblast function in tissue repair and disease.

3.8. Fluorescence Imaging of NAD(P)H in *Drosophila* Larvae. We explored the application of probe **A** for *in vivo* detection of NADH levels in fruit fly larvae (*Drosophila melanogaster*), using a controlled experimental setup to ensure reproducibility.[9,21,55] Starvation was employed as a strategy to deplete endogenous NADH levels, providing a consistent and low baseline for subsequent NADH treatments.[9,21,55] This approach allowed us to more accurately assess the probe's sensitivity and specificity in detecting exogenously introduced NADH. Starved, newly hatched larvae were incubated in a pH 7.4 phosphate-buffer at diverse concentrations of NADH for 2 h. This step enabled the larvae to uptake and accumulate NADH in a controlled manner. After the incubation period, the larvae were thoroughly washed to remove any unbound NADH, ensuring that subsequent emission measurements reflected intracellular NADH levels rather than extracellular remnants. The larvae were then exposed to 10 μM probe **A** in a PBS with for an extra 2 h. allowing sufficient time for the probe to permeate the larvae and interact with intracellular NADH (Figure 11). The emission images revealed a distinct correlation between NADH concentration and emission intensity in the larvae. In the control group (0 μM NADH), insignificant emission was observed, consistent with the low NADH levels expected under starvation conditions. As the concentration of NADH increased, an associated increase in emission intensity was detected, indicating successful detection of NADH by probe **A**. The emission intensity was most pronounced in the larvae treated with 80 μM NADH, demonstrating the probe's capacity to distinguish between different NADH concentrations. These results confirm the efficiency of probe **A** in determining NADH in a live organism, with a clear dose-dependent fluorescence response. Moreover, the use of starved larvae as a control highlighted the probe's selectivity. The insignificant fluorescence observed in the lack of exogenous NADH suggests that probe **A** does not significantly interact with other intracellular components under these conditions, further validating its specificity for NADH. This ability to monitor NADH levels in vivo is particularly valuable for studying metabolic processes, cellular redox states, and the effects of external stimuli on NADH dynamics.

To evaluate the capability of probe **A** to determine glucose-induced changes in NADH levels *in vivo*, we conducted fluorescence imaging studies using newly hatched, food-

https://doi.org/10.1021/acsabm.4c01294
ACS Appl. Bio Mater. 2024, 7, 8465−8478

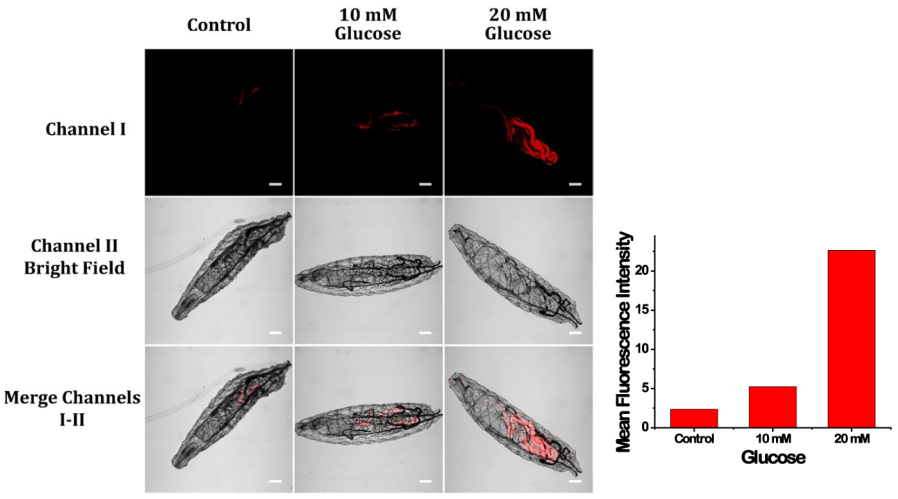

Figure 12. Emission images of newly hatched, nutrient-deprived fruit fly larvae exposed to various glucose levels in pH 7.4 phosphate-buffer for 2 h. Afterward, the larvae were cleaned thrice with PBS and further treated with probe **A** at 10 μM in PBS for extra 2 h. Emission was imaged in the 650−750 nm range with 559 nm excitation.

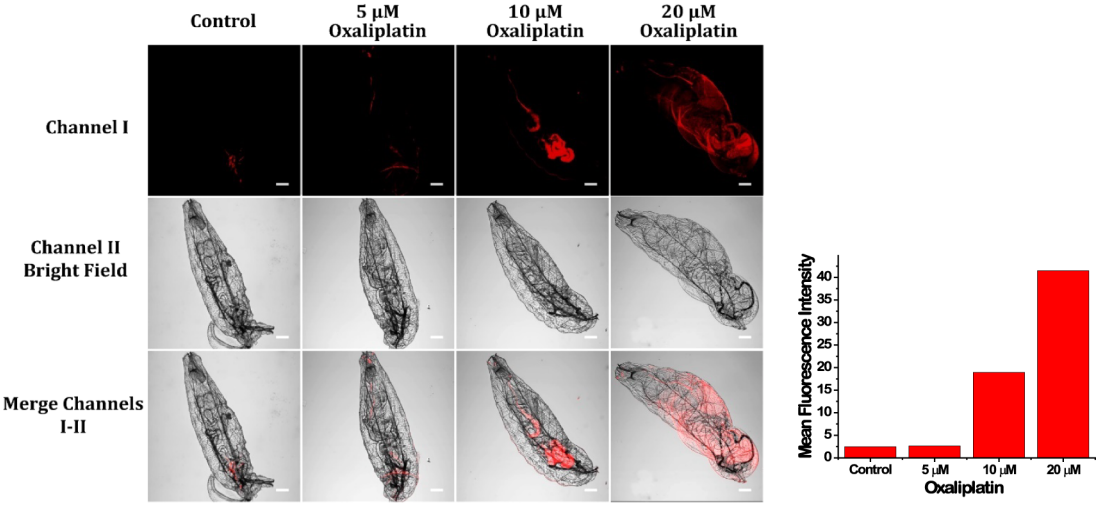

Figure 13. Emission imaging of newly hatched, nutrient-deprived fruit fly larvae exposed to diverse concentrations of oxaliplatin in pH 7.4 phosphate-buffer for 2 h. After incubation, the larvae were cleaned thrice with PBS and then dipped in a PBS solution with 10 μM probe **A** for an extra 2 h. Emission was imaged in the 650−750 nm range with 559 nm excitation.

deprived fruit fly larvae. Starvation was employed as a strategy to reduce the larvae's endogenous glucose and NADH levels,[9,21,55] establishing a low baseline for the subsequent glucose treatments. The larvae were suspended in PBS buffer at pH 7.4, containing glucose concentrations of 0 mM (control), 10 mM, and 20 mM, for a duration of 2 h. This incubation allowed the larvae to metabolize the glucose, leading to an increase in intracellular NADH levels as glucose metabolism progressed. After incubation, the larvae were thoroughly cleaned with PBS to remove any residual glucose, ensuring that the emission signals observed were due to intracellular processes. After washing, the larvae were treated with a PBS solution with 10 μM probe **A** for an extra 2 h. This allowed the probe to interact with the NADH produced within the larvae (Figure 12). The emission imaging results revealed a clear correlation between glucose concentration and fluorescence intensity in the larvae. The control group (0 mM glucose) exhibited minimal fluorescence, reflecting the low NADH levels expected under starvation conditions. In contrast, larvae incubated with 10 mM and 20 mM glucose displayed progressively higher emission intensities, corresponding to the increased intracellular NADH levels resulting from glucose metabolism. The increase in emission intensity with enhanced glucose concentrations showcases the sensitivity of probe **A** in detecting NADH levels within living organisms. The probe's sensitivity to NADH produced through glucose metabolism highlights its potential for studying metabolic pathways and energy production *in vivo*. Additionally, the minimal fluorescence observed in the control group underscores the specificity of probe **A** for NADH, as the probe did not generate significant signals in the absence of glucose-induced NADH production. Overall, these findings underscore the utility of probe **A** for monitoring glucose metabolism and its impact on NADH levels in live organisms. This approach can be extended to other metabolic studies, where real-time monitoring of NADH levels is critical for understanding the effects of various metabolic interventions or disease conditions.

Oxaliplatin, a chemotherapeutic drug incorporating platinum, is extensively utilized for treating different types of cancers, with a particular focus on colorectal cancer.[56−61] It

https://doi.org/10.1021/acsabm.4c01294
ACS Appl. Bio Mater. 2024, 7, 8465−8478

primarily works by inducing DNA cross-linking, disrupting DNA replication and transcription, and ultimately causing cell death. However, oxaliplatin's effects are not limited to DNA damage.[56−61] It is also known to impact cellular metabolism and induce oxidative stress, which can result in alterations in NADH levels, a crucial cofactor participating in cellular redox reactions and ATP synthesis.[56−61] To examine the effects of oxaliplatin on NADH levels *in vivo*, we conducted fluorescence imaging studies using freshly hatched, nutrient-deprived fruit fly larvae. The larvae were starved to reduce endogenous NADH levels, ensuring that any observed changes in emission could be attributed to the drug treatment.[9,21,51,55] The larvae were treated with oxaliplatin with diverse concentrations in PBS solution with a pH of 7.4 for 2 h. After the incubation period, the larvae were thoroughly cleaned to remove residual oxaliplatin and then placed in a PBS solution with 10 μM probe **A** for an extra 2 h. Probe **A** is specifically designed to detect NADH, providing a means to monitor the metabolic impact of oxaliplatin in the larvae (Figure 13). The results indicated that treatment with 5 μM oxaliplatin did not cause a significant increase in emission in contrast to the control group, suggesting that this lower concentration may not significantly affect NADH levels. In contrast, treatment with 10 μM and 20 μM oxaliplatin resulted in substantial increases in fluorescence intensity, demonstrating a clear dose-dependent relationship. This finding implies that higher concentrations of oxaliplatin induce significant changes in cellular metabolism, possibly due to increased oxidative stress or disruptions in mitochondrial function, which, in turn, elevate NADH levels. The observed dose-dependent fluorescence increase highlights the broader biological effects of oxaliplatin beyond its DNA-damaging capabilities, providing crucial understanding of its influence on cellular metabolism. In summary, this study demonstrates the potential of probe **A** for real-time, *in vivo* assessment of NADH changes in response to oxaliplatin treatment. The observed metabolic alterations in fruit fly larvae at higher oxaliplatin concentrations reflect the drug's capacity to disrupt cellular processes, emphasizing the importance of integrating metabolic considerations into the evaluation of chemotherapeutic effectiveness and side effects.

3.9. Investigating NAD(P)H Levels in ADPKD Using Fluorescent Probe A. Autosomal dominant polycystic kidney disease (ADPKD) is defined by a multifaceted set of pathophysiological changes that disturb normal metabolic functions. These changes often involve dysregulated cellular mechanisms, such as increased glycolysis, mitochondrial dysfunction, oxidative stress, inflammation, and hypoxia. Such metabolic alterations can lead to elevated levels of NADH and NADPH in the kidney tissues of affected individuals, indicating significant shifts in cellular energy dynamics and redox states. In this study, we employed fluorescent probe **A** to investigate NAD(P)H levels in the kidneys of both ADPKD mouse models and human patients. We specifically compared renal NAD(P)H levels between 5-week-old phenotypic wildtype (WT, $Pkd1^{RC/+}$) mice and those with ADPKD ($Pkd1^{RC/RC}$). Our findings revealed that the kidneys of WT mice exhibited minimal fluorescence, suggesting lower NAD(P)H levels, while the cystic kidneys of ADPKD mice displayed markedly increased fluorescence, indicating elevated NAD(P)H concentrations relative to their healthy counterparts (Figure S16). Furthermore, we observed that human ADPKD kidneys showed higher NAD(P)H levels compared to age- and sex-matched normal human kidneys (NHK). These results demonstrate the effectiveness of probe **A** in identifying metabolic differences associated with kidney diseases, providing critical insights into the underlying mechanisms of ADPKD and pointing to potential therapeutic targets (Figure S17). By clarifying these metabolic changes, this study enhances our understanding of ADPKD pathophysiology and lays the groundwork for developing targeted interventions aimed at restoring metabolic balance and improving clinical outcomes for ADPKD patients.

4. CONCLUSION

In this study, we introduce a near-infrared emissive probe tailored for sensitive detection of NAD(P)H in complex biological environments. Utilizing the advantageous properties of coumarin-based fluorophores, our probe integrates a NAD(P)H-sensitive 3-quinolinium acceptor with a coumarin dye through a vinyl linkage. This design effectively mitigates fluorescence interference from NADH and leverages the high molar absorptivity and outstanding photostability of coumarin derivatives. Our findings validate the probe's exceptional performance in monitoring NAD(P)H dynamics with both high sensitivity and specificity. The probe successfully detected changes in NAD(P)H levels within HeLa cells under various circumstances. Notably, glucose and maltose treatments brought about emission increases due to enhanced NAD(P)H levels, highlighting the probe's ability to discern metabolic changes. The probe demonstrated specificity for mitochondria enabled detailed investigations into mitochondrial metabolism and function under various metabolic conditions and stress responses. Its mitochondrial specificity and sensitivity to NAD(P)H levels offer considerable potential for advancing research into mitochondrial physiology and related pathophysiological conditions. In our investigation of NAD(P)H levels in ADPKD using fluorescent probe **A**, we observed higher NAD(P)H concentrations in the cystic kidneys of ADPKD mouse models and human patients compared to healthy controls, further underscoring the probe's effectiveness in detecting metabolic alterations associated with kidney disease. Additional validation in nutrient-deprived fruit fly larvae reinforced the probe's applicability in living organisms. The observed emission responses to varying concentrations of NADH, glucose, maltose, cisplatin, and fludarabine underscore its robust applicability across cellular and whole-organism models. Overall, this near-infrared emissive probe represents a significant advancement in real-time NAD(P)H monitoring. Its capacity to deliver accurate, high-resolution data on NAD(P)H fluctuations makes it a valuable tool for in-depth studies of cellular metabolism and therapeutic effects. By minimizing background interference and enhancing sensitivity, the probe opens new avenues for exploring NAD(P)H dynamics and its implications in health and disease. This advancement promises to deepen our knowledge of metabolic processes and improve the evaluation of drug responses, paving the way for future research and clinical applications.

■ ASSOCIATED CONTENT

Supporting Information

The Supporting Information is available free of charge at https://pubs.acs.org/doi/10.1021/acsabm.4c01294.

Comprehensive descriptions of the instrumentation and reagents used, along with the synthesis of probe **A** and its precursors; detailed NMR and MS spectra for the

https://doi.org/10.1021/acsabm.4c01294
ACS Appl. Bio Mater. 2024, 7, 8465−8478

intermediates and probe **A** are provided, as well as the MS spectra of the product formed from the probe's interaction with NADH; additional data includes time-dependent fluorescence measurements for probe **A**, an analysis of the linear fluorescence responses to varying NADH concentrations, and assessments of the probe's photostability and selectivity; the methodologies for culturing HeLa cells and the imaging of *Drosophila melanogaster* larvae to evaluate probe efficacy in biological systems; results from the MTT assay to assess cell viability following treatment, alongside theoretical calculations that support the experimental findings (PDF)

AUTHOR INFORMATION

Corresponding Authors

Sushil K. Dwivedi − *Department of Chemistry, Michigan Technological University, Houghton, Michigan 49931, United States; Health Research Institute, Michigan Technological University, Houghton, Michigan 49931, United States*; Email: sdwive2@mtu.edu

Yan Zhang − *Department of Biological Sciences, Michigan Technological University, Houghton, Michigan 49931, United States*; Email: yzhang51@mtu.edu

Athar Ata − *Department of Chemistry, Michigan Technological University, Houghton, Michigan 49931, United States; Health Research Institute, Michigan Technological University, Houghton, Michigan 49931, United States*; Email: aata@mtu.edu

Rudy L Luck − *Department of Chemistry, Michigan Technological University, Houghton, Michigan 49931, United States*; orcid.org/0000-0001-5436-1942; Email: rluck@mtu.edu

Haiying Liu − *Department of Chemistry, Michigan Technological University, Houghton, Michigan 49931, United States; Health Research Institute, Michigan Technological University, Houghton, Michigan 49931, United States*; orcid.org/0000-0001-8351-2017; Email: hyliu@mtu.edu

Authors

Sophia Jaeger − *Department of Chemistry, Michigan Technological University, Houghton, Michigan 49931, United States; Health Research Institute, Michigan Technological University, Houghton, Michigan 49931, United States*

Henry Lanquaye − *Department of Chemistry, Michigan Technological University, Houghton, Michigan 49931, United States; Health Research Institute, Michigan Technological University, Houghton, Michigan 49931, United States*

Dilka Liyana Arachchige − *Department of Chemistry, Michigan Technological University, Houghton, Michigan 49931, United States; Health Research Institute, Michigan Technological University, Houghton, Michigan 49931, United States*

James Xia − *Woodbury high school, Woodbury, Minnesota 55125, United States*

May Waters − *Department of Chemistry, Michigan Technological University, Houghton, Michigan 49931, United States; Health Research Institute, Michigan Technological University, Houghton, Michigan 49931, United States*

Bella Lyn Bigari − *Department of Biological Sciences, Michigan Technological University, Houghton, Michigan 49931, United States*

Adenike Mary Olowolagba − *Department of Chemistry, Michigan Technological University, Houghton, Michigan 49931, United States; Health Research Institute, Michigan Technological University, Houghton, Michigan 49931, United States*

Peter Agyemang − *Department of Chemistry, Michigan Technological University, Houghton, Michigan 49931, United States; Health Research Institute, Michigan Technological University, Houghton, Michigan 49931, United States*

Yang Zhang − *Department of Biological Sciences, Michigan Technological University, Houghton, Michigan 49931, United States*

Ishana Kathuria − *Department of Chemistry, Michigan Technological University, Houghton, Michigan 49931, United States*

Thomas Werner − *Department of Biological Sciences, Michigan Technological University, Houghton, Michigan 49931, United States*

Complete contact information is available at: https://pubs.acs.org/10.1021/acsabm.4c01294

Author Contributions

S.J., H.L., D.L.A., and S.K.D. contributed to investigation, methodology, data curation, and formal analysis; S.K.D. also supervised graduate and undergraduate students; M.W., J.X., A.M.O., and P.A. provided validation; B.L.B. and Y.Z. focused on data curation; I.K. specialized in computational chemistry; A.A. and T.W. supervised and edited the manuscript; and Y.Z., R.L.L., and H.L. managed funding acquisition, project administration, conceptualization, and manuscript preparation and editing.

Notes

The authors declare no competing financial interest.

ACKNOWLEDGMENTS

This research was supported by a range of funding sources. Y. Zhang received grants from the National Institute of Diabetes and Digestive and Kidney Diseases (Award Number R15DK137195) and the PKD Foundation (Grant 1021264). She expresses her gratitude to the Kansas PKD Research and Translation Core Center at the University of Kansas Medical Center (U54D126126) and the Polycystic Kidney Disease Research Resource Consortium (PKD-RRC) for providing essential kidney sections from human ADPKD and normal human kidneys. Furthermore, the National Institute of General Medical Sciences at the National Institutes of Health provided significant funding through Award Numbers R15 GM146206-01 and two supplemental grants to H. Liu as principal investigator and R. L. Luck as coprincipal investigator. This funding enabled the acquisition of a cell incubator with oxygen level control and an LC−MS system. We also acknowledge the National Science Foundation for its support under Award Number 2117318, which facilitated the purchase of a new NMR spectrometer crucial for the structural characterization of intermediates and probes, with H. Liu as the grant recipient. The analysis of the fluorescent probe was conducted with support from the high-performance computing facilities at Michigan Technological University. We sincerely thank these

organizations for their critical support, which was instrumental in the successful completion of this research.

REFERENCES

(1) Berthiaume, J. M.; Kurdys, J. G.; Muntean, D. M.; Rosca, M. G. Mitochondrial NAD+, NADH Redox State and Diabetic Cardiomyopathy. *Antioxid. Redox Signal.* **2019**, *30* (3), 375−398.
(2) Goodman, R. P.; Calvo, S. E.; Mootha, V. K. Spatiotemporal compartmentalization of hepatic NADH and NADPH metabolism. *J. Biol. Chem.* **2018**, *293* (20), 7508−7516.
(3) Liszewska, A.; Robak, E.; Bernacka, M.; Bogaczewicz, J.; Wozniacka, A. Methotrexate use and NAD+/NADH metabolism in psoriatic keratinocytes. *Postepy Dermatologii I Alergologii* **2020**, *37* (1), 19−22.
(4) Winkler, U.; Hirrlinger, J. Crosstalk of Signaling and Metabolism Mediated by the NAD+/NADH Redox State in Brain Cells. *Neurochem. Res.* **2015**, *40* (12), 2394−2401.
(5) Yan, L. J. NADH/NAD+ Redox Imbalance and Diabetic Kidney Disease. *Biomolecules* **2021**, *11* (5), 730.
(6) Ying, W. H. NAD+ and NADH in cellular functions and cell death. *Front. Biosci.-Landmark* **2006**, *11*, 3129−3148.
(7) Park, S. Y.; Yoon, S. A.; Cha, Y. J.; Lee, M. H. Recent advances in fluorescent probes for cellular antioxidants: Detection of NADH, hNQO1, H_2S, and other redox biomolecules. *Coord. Chem. Rev.* **2021**, *428*, 213613.
(8) Sun, P. J.; Zhang, H. X.; Sun, Y. Q.; Liu, J. The recent development of fluorescent probes for the detection of NADH and NADPH in living cells and *in vivo*. *Spectrochim. Acta, Part A* **2021**, *245*, 118919.
(9) Dwivedi, S. K.; Arachchige, D. L.; Waters, M.; Jaeger, S.; Mahmoud, M.; Olowolagba, A. M.; Tucker, D. R.; Geborkoff, M. R.; Werner, T.; Luck, R. L. Near-infrared absorption and emission probes with optimal connection bridges for live monitoring of NAD(P)H dynamics in living systems. *Sens. Actuators, B* **2024**, *402*, 135073.
(10) Hong, S. N.; Pawel, G. T.; Pei, R. J.; Lu, Y. Recent progress in developing fluorescent probes for imaging cell metabolites. *Biomed. Mater.* **2021**, *16* (4), 044108.
(11) Li, M. Z.; Liu, C.; Zhang, W. J.; Xu, L. F.; Yang, M. M.; Chen, Z. L.; Wang, X. X.; Pu, L. L.; Liu, W. L.; Zeng, X. S. An NADH-selective and sensitive fluorescence probe to evaluate living cell hypoxic stress. *J. Mater. Chem. B* **2021**, *9* (46), 9547−9552.
(12) Podder, A.; Koo, S.; Lee, J.; Mun, S.; Khatun, S.; Kang, H. G.; Bhuniya, S.; Kim, J. S. A rhodamine based fluorescent probe validates substrate and cellular hypoxia specific NADH expression. *Chem. Commun.* **2019**, *55* (4), 537−540.
(13) Podder, A.; Murali, V. P.; Deepika, S.; Dhamija, A.; Biswas, S.; Maiti, K. K.; Bhuniya, S. NADH-Activated Dual-Channel Fluorescent Probes for Multicolor Labeling of Live Cells and Tumor Mimic Spheroids. *Anal. Chem.* **2020**, *92* (18), 12356−12362.
(14) Podder, A.; Thirumalaivasan, N.; Chao, Y. K.; Kukutla, P.; Wu, S. P.; Bhuniya, S. Two-photon active fluorescent indicator for detecting NADH dynamics in live cells and tumor tissue. *Sens. Actuators, B* **2020**, *324*, 128637.
(15) Sharma, H.; Tan, N. K.; Trinh, N.; Yeo, J. H.; New, E. J.; Pfeffer, F. M. A fluorescent naphthalimide NADH mimic for continuous and reversible sensing of cellular redox state. *Chem. Commun.* **2020**, *56* (15), 2240−2243.
(16) Sun, Y. X.; Mao, Y. Y.; Bai, T. W.; Ye, T. Q.; Lin, Y. F.; Wang, F.; Li, L.; Guo, L. H.; Liu, H. Y.; Wang, J. B. An activated near-infrared mitochondrion-targetable fluorescent probe for rapid detection of NADH. *Chem. Commun.* **2024**, *60* (46), 5932−5935.
(17) Wang, L.; Zhang, J. Y.; Kim, B.; Peng, J. J.; Berry, S. N.; Ni, Y.; Su, D. D.; Lee, J.; Yuan, L.; Chang, Y. T. Boronic Acid: A Bio-Inspired Strategy To Increase the Sensitivity and Selectivity of Fluorescent NADH Probe. *J. Am. Chem. Soc.* **2016**, *138* (33), 10394−10397.
(18) Wang, Q.; Zhu, Y. Z.; Chen, D. B.; Ou, J. L.; Chen, M.; Feng, Y.; Wang, W. B.; Meng, X. M. A dual-salt fluorescent probe for specific recognition of mitochondrial NADH and potential cancer diagnosis. *Talanta* **2023**, *257*, 124393.
(19) Zhang, Y. B.; Arachchige, D. L.; Olowolagba, A.; Luck, R. L.; Liu, H. Y. Near-infrared fluorescent probe based on rhodamine derivative for detection of NADH in live cells. *Methods* **2022**, *204*, 22−28.
(20) Dai, F.; Zhang, S. X.; Zhou, B.; Duan, D. C.; Liu, J. R.; Zheng, Y. L.; Chen, H.; Zhang, X. Y.; Zhang, Y. Cellular and Intravital Imaging of NAD(P)H by a Red-Emitting Quinolinium-Based Fluorescent Probe that Features a Shift of Its Product from Mitochondria to the Nucleus. *Anal. Chem.* **2022**, *95* (2), 1335−1342.
(21) Arachchige, D. L.; Dwivedi, S. K.; Waters, M.; Jaeger, S.; Peters, J.; Tucker, D. R.; Geborkoff, M.; Werner, T.; Luck, R. L.; Godugu, B. Sensitive monitoring of NAD(P)H levels within cancer cells using mitochondria-targeted near-infrared cyanine dyes with optimized electron-withdrawing acceptors. *J. Mater. Chem. B* **2024**, *12* (2), 448−465.
(22) Fomin, M. A.; Dmitriev, R. I.; Jenkins, J.; Papkovsky, D. B.; Heindl, D.; König, B. Two-Acceptor Cyanine-Based Fluorescent Indicator for NAD(P)H in Tumor Cell Models. *ACS Sens.* **2016**, *1* (6), 702−709.
(23) Ma, K. Q.; Yang, H.; Wu, X. K.; Huo, F. J.; Cheng, F. Q.; Yin, C. X. An Activatable NIR Fluorescent Probe for NAD(P)H and Its Application to the Real-Time Monitoring of p53 Abnormalities In Vivo. *Angew. Chem., Int. Ed.* **2023**, *62* (19), No. e202301518.
(24) Zhao, Y. H.; Wei, K. Y.; Kong, F. P.; Gao, X. N.; Xu, K. H.; Tang, B. Dicyanoisophorone-Based Near-Infrared-Emission Fluorescent Probe for Detecting NAD(P)H in Living Cells and in Vivo. *Anal. Chem.* **2019**, *91* (2), 1368−1374.
(25) Cao, D. X.; Liu, Z. Q.; Verwilst, P.; Koo, S.; Jangjili, P.; Kim, J. S.; Lin, W. Y. Coumarin-Based Small-Molecule Fluorescent Chemosensors. *Chem. Rev.* **2019**, *119* (18), 10403−10519.
(26) Das, S.; Indurthi, H. K.; Saha, P.; Sharma, D. K. Coumarin-based fluorescent probes for the detection of ions, biomolecules and biochemical species responsible for diseases. *Dyes Pigm.* **2024**, *228*, 112257.
(27) Fan, Y. F.; Wu, Y.; Hou, J.; Wang, P.; Peng, X. J.; Ge, G. B. Coumarin-based near-infrared fluorogenic probes: Recent advances, challenges and future perspectives. *Coord. Chem. Rev.* **2023**, *480*, 215020.
(28) Sun, X. Y.; Liu, T.; Sun, J.; Wang, X. J. Synthesis and application of coumarin fluorescence probes. *RSC Adv.* **2020**, *10* (18), 10826−10847.
(29) Szwaczko, K. Fluorescent Coumarin-based Probe for Detection of Biological Thiols. *Curr. Org. Chem.* **2023**, *27* (15), 1329−1335.
(30) Dai, H.; Deng, Z. Y.; Zeng, Y. B.; Zhang, J.; Yang, Y. W.; Ma, Q. Y.; Hu, W. L.; Guo, L. H.; Li, L.; Wan, S. L. Highly sensitive determination of 4-nitrophenol with coumarin-based fluorescent molecularly imprinted poly (ionic liquid). *J. Hazard. Mater.* **2020**, *398*, 122854.
(31) Fang, M. X.; Adhikari, R.; Bi, J. H.; Mazi, W.; Dorh, N.; Wang, J. B.; Conner, N.; Ainsley, J.; Karabencheva-Christova, T. G.; Luo, F. T. Fluorescent probes for sensitive and selective detection of pH changes in live cells in visible and near-infrared channels. *J. Mater. Chem. B* **2017**, *5* (48), 9579−9590.
(32) Olowolagba, A. M.; Idowu, M. O.; Arachchige, D. L.; Aworinde, O. R.; Dwivedi, S. K.; Graham, O. R.; Werner, T.; Luck, R. L.; Liu, H. Y. Syntheses and Applications of Coumarin-Derived Fluorescent Probes for Real-Time Monitoring of NAD(P)H Dynamics in Living Cells across Diverse Chemical Environments. *ACS Appl. Bio Mater.* **2024**, *7*, 5437.
(33) Wan, S. L.; Xia, S.; Medford, J.; Durocher, E.; Steenwinkel, T. E.; Rule, L.; Zhang, Y. B.; Luck, R. L.; Werner, T.; Liu, H. Y. A ratiometric near-infrared fluorescent probe based on a novel reactive cyanine platform for mitochondrial pH detection. *J. Mater. Chem. B* **2021**, *9* (25), 5150−5161.
(34) Xia, S.; Wang, J. B.; Bi, J. H.; Wang, X.; Fang, M. X.; Phillips, T.; May, A.; Conner, N.; Tanasova, M.; Luo, F. T. Fluorescent probes based on π-conjugation modulation between hemicyanine and coumarin moieties for ratiometric detection of pH changes in live

https://doi.org/10.1021/acsabm.4c01294
ACS Appl. Bio Mater. 2024, 7, 8465−8478

cells with visible and near-infrared channels. *Sens. Actuators, B* **2018**, *265*, 699−708.
(35) Xia, S.; Zhang, Y. B.; Fang, M. X.; Mikesell, L.; Steenwinkel, T. E.; Wan, S. L.; Phillips, T.; Luck, R. L.; Werner, T.; Liu, H. Y. A FRET-Based Near-Infrared Fluorescent Probe for Ratiometric Detection of Cysteine in Mitochondria. *ChemBiochem* **2019**, *20* (15), 1986−1994.
(36) Zhang, Y. B.; Qiu, X. Y.; Sun, L.; Yan, Q.; Luck, R. L.; Liu, H. Y. A two-photon fluorogenic probe based on a coumarin schiff base for formaldehyde detection in living cells. *Spectrochim. Acta, Part A* **2022**, *274*, 121074.
(37) Zhang, Y. B.; Xia, S.; Wan, S. L.; Steenwinkel, T. E.; Vohs, T.; Luck, R. L.; Werner, T.; Liu, H. Y. Ratiometric Detection of Glutathione Based on Disulfide Linkage Rupture between a FRET Coumarin Donor and a Rhodamine Acceptor. *ChemBiochem* **2021**, *22* (13), 2282−2291.
(38) Zhang, Y. B.; Yan, Y. N.; Xia, S.; Wan, S. L.; Steenwinkel, T. E.; Medford, J.; Durocher, E.; Luck, R. L.; Werner, T.; Liu, H. Y. Cell Membrane-Specific Fluorescent Probe Featuring Dual and Aggregation-Induced Emissions. *ACS Appl. Mater. Interfaces* **2020**, *12* (18), 20172−20179.
(39) *Gaussian 16, Revision A.03*; Gaussian, Inc.: Wallingford CT, 2016.
(40) Austin, A.; Petersson, G. A.; Frisch, M. J.; Dobek, F. J.; Scalmani, G.; Throssell, K. A Density Functional with Spherical Atom Dispersion Terms. *J. Chem. Theory Comput.* **2012**, *8* (12), 4989−5007.
(41) Mazi, W.; Yan, Y. N.; Zhang, Y. B.; Xia, S.; Wan, S. L.; Tajiri, M.; Luck, R. L.; Liu, H. Y. A near-infrared fluorescent probe based on a hemicyanine dye with an oxazolidine switch for mitochondrial pH detection. *J. Mater. Chem. B* **2021**, *9* (3), 857−863.
(42) Zhang, S. W.; Chen, T. H.; Lee, H. M.; Bi, J. H.; Ghosh, A.; Fang, M. X.; Qian, Z. C.; Xie, F.; Ainsley, J.; Christov, C.; Luo, F.-T. Luminescent Probes for Sensitive Detection of pH Changes in Live Cells through Two Near-Infrared Luminescence Channels. *ACS Sens.* **2017**, *2* (7), 924−931.
(43) Zhang, Y. B.; Hu, J.; Rong, X. Q.; Jiang, J.; Wang, Y.; Zhang, X. T.; Xu, Z. H.; Xu, K.; Wu, M.; Fang, M. X. Development of a hybrid rhodamine-hydrazine NIR fluorescent probe for sensitive detection and imaging of peroxynitrite in necrotizing enterocolitis model. *Bioorg. Chem.* **2024**, *152*, 107729.
(44) Shang, J. T.; Zhang, Y. Y.; Cheng, Y. T.; Wang, B. L.; Rong, X. Q.; Zhang, Y. B.; Gao, W.; Fang, M. X. Development of a novel Near-Infrared fluorescent probe based on rhodamine derivative for highly selective and sensitive detection of phosgene. *Microchem. J.* **2024**, *196*, 109653.
(45) Zhang, Y. B.; Wang, S. C.; Sun, Y.; Xu, H. B.; Xu, Z. H.; Liang, X.; Yang, J. G.; Song, W. Y.; Chen, M. H.; Fang, M. X. Evaluation of a biomarker (NO) dynamics in inflammatory zebrafish and periodontitis saliva samples via a fast-response and sensitive fluorescent probe. *Bioorg. Chem.* **2024**, *143*, 107014.
(46) Fang, M. X.; Zhou, X. Y.; Wang, S. C.; Yang, Y. S.; Cheng, Y. T.; Wang, B. L.; Rong, X. Q.; Zhang, X. L.; Xu, K.; Zhang, Y. B.; et al. A novel near-infrared fluorescent probe with hemicyanine scaffold for sensitive mitochondrial pH detection and mitophagy study. *Spectrochim. Acta, Part A* **2023**, *298*, 122791.
(47) Circu, M. L.; Maloney, R. E.; Aw, T. Y. Low glucose stress decreases cellular NADH and mitochondrial ATP in colonic epithelial cancer cells: Influence of mitochondrial substrates. *Chem.-Biol. Interact.* **2017**, *264*, 16−24.
(48) Elter, T.; Hallek, M.; Engert, A. Fludarabine in chronic lymphocytic leukaemia. *Expert Opin. Pharmacother.* **2006**, *7* (12), 1641−1651.
(49) Lukenbill, J.; Kalaycio, M. Fludarabine: A review of the clear benefits and potential harms. *Leuk. Res.* **2013**, *37* (9), 986−994.
(50) Montillo, M.; Ricci, F.; Tedeschi, A. Role of fludarabine in hematological malignancies. *Expert Rev. Anticancer Ther.* **2006**, *6* (9), 1141−1161.
(51) Barabas, K.; Milner, R.; Lurie, D.; Adin, C. Cisplatin: a review of toxicities and therapeutic applications. *Vet. Comp. Oncol.* **2008**, *6* (1), 1−18.
(52) Crona, D. J.; Faso, A.; Nishijima, T. F.; McGraw, K. A.; Galsky, M. D.; Milowsky, M. I. A Systematic Review of Strategies to Prevent Cisplatin-Induced Nephrotoxicity. *Oncologist* **2017**, *22* (5), 609−619.
(53) Li, Y. R.; Zhang, T. Y.; Song, Q.; Gao, D. K.; Li, Y.; Jie, H. Q.; Huang, P.; Zheng, G. L.; Yang, J.; He, J. C. Cisplatin ototoxicity mechanism and antagonistic intervention strategy: a scope review. *Front. Cell Neurosci.* **2023**, *17*, 1−12.
(54) Yao, X.; Panichpisal, K.; Kurtzman, N.; Nugent, K. Cisplatin nephrotoxicity: A review. *Am. J. Med. Sci.* **2007**, *334* (2), 115−124.
(55) Dwivedi, S. K.; Arachchige, D. L.; Olowolagba, A.; Mahmoud, M.; Cunnien, J.; Tucker, D. R.; Fritz, D.; Werner, T.; Luck, R. L.; Liu, H. Y. Thiophene-based organic dye with large Stokes shift and deep red emission for live cell NAD(P)H detection under varying chemical stimuli. *J. Mater. Chem. B* **2023**, *11* (27), 6296−6307.
(56) Alcindor, T.; Beauger, N. Oxaliplatin: a review in the era of molecularly targeted therapy. *Curr. Oncol.* **2011**, *18* (1), 18−25.
(57) Argyriou, A. A.; Polychronopoulos, P.; Iconomou, G.; Chroni, E.; Kalofonos, H. P. A review on oxaliplatin-induced peripheral nerve damage. *Cancer Treat. Rev.* **2008**, *34* (4), 368−377.
(58) Montagnani, F.; Turrisi, G.; Marinozzi, C.; Aliberti, C.; Fiorentini, G. Effectiveness and safety of oxaliplatin compared to cisplatin for advanced, unresectable gastric cancer: a systematic review and meta-analysis. *Gastric Cancer* **2011**, *14* (1), 50−55.
(59) Pasetto, L. M.; D'Andrea, M. R.; Rossi, E.; Monfardini, S. Oxaliplatin-related neurotoxicity: How and why? *Crit. Rev. Oncol. Hematol.* **2006**, *59* (2), 159−168.
(60) Raymond, E.; Chaney, S. G.; Taamma, A.; Cvitkovic, E. Oxaliplatin: A review of preclinical and clinical studies. *Ann. Oncol.* **1998**, *9* (10), 1053−1071.
(61) Stein, A.; Arnold, D. Oxaliplatin: a review of approved uses. *Expert Opin. Pharmacother.* **2012**, *13* (1), 125−137.

https://doi.org/10.1021/acsabm.4c01294
ACS Appl. Bio Mater. 2024, 7, 8465−8478